PATENT-RELATED CONFIDENTAL INFORMATION

PLEASE DO NOT DISCLOSE OR DISTRIBUTE

T-CELL MEMBRANE CAMOUFLAGED NANOPARTICLES FOR TREATMENT OF MELANOMA

by

GIZEM OTER

Presented to the Faculty of the Graduate School of

The University of Texas at Arlington in Partial Fulfillment

of the Requirements

for the Degree of

MASTER OF SCIENCE IN BIOMEDICAL ENGINEERING

THE UNIVERSITY OF TEXAS AT ARLINGTON

May 2017

Acknowledgements

My deepest gratitude goes first and foremost to my advisors, Dr. Kytai T. Nguyen and Dr. Jon Weidanz for their constant guidance, encouragement, and patience during the period of my Master's project. Without them and the knowledge they have passed on to me, this work could not be completed. I am grateful to them for giving me an opportunity to work in their laboratories as a graduate student. I would like to extend my appreciation and gratitude to Dr. Ashwin Nair and Dr. Justyn Jaworski for serving as my thesis committee member.

Similarly, not very much of this would have been possible without the support of my wonderful mentor, Daria Zhukova. She has been a great influence on me and has guided me in developing into a researcher that I am today. I am appreciative of having had the opportunity to work with her, and believe that we have made a great team over the years. Also, very special thanks go to Dr. Manoj K. Sabnani, who assisted and mentored us about flow cytometry, Western blot and binding studies in this project. I am grateful for all of his patience, kindness and support. Moreover, I am greatly indebted to all my laboratory colleagues and it is an honor for me to share my memories of the work in Dr. Nguyen's laboratory with them.

Finally, all thanks go to my family and government guidance. They have been crucial to my emotional and financial stability during these two years. I could not do it without them and the support that they have provided me throughout this journey.

May 10, 2017

ABSTRACT

T-CELL MEMBRANE CAMOUFLAGED NANOPARTICLES

FOR TREATMENT OF MELANOMA

Gizem Oter, MS

The University of Texas at Arlington, 2017

Supervising Professor: Kytai Truong Nguyen, Jon Weidanz

Melanoma is one of the most aggressive skin cancers. The American Cancer Society reports that every hour, one person dies from melanoma. While there are a number of treatments currently available for melanoma (e.g. surgery, chemotherapy, immunotherapy, radiation therapy), these therapies face several problems, including inadequate response rates, high toxicity, and severe side effects due to non-specific delivery of anti-cancer drugs. To improve therapeutic efficiency and reduce these limitations, a multifunctional nanoparticle has been developed. Specifically, poly (lactic-co-glycolic acid) (PLGA) nanoparticles (NPs) were coated with a cellular membrane derived from the T cell hybridoma, 19LF6 endowed with a melanoma-specific anti-gp100/ HLA-A2 T-cell receptor (TCR) and loaded with an FDA-approved melanoma chemotherapeutic drug Trametinib. These NPs were hypothesized to have improved stealth and targeting capabilities against skin cancer cells.

T-cell membrane camuflaged trametinib loaded PLGA NPs displayed a negative average zeta potential of -36 mV and an average size of 246 nm. The particles were found to be stable for at least 2 days in 90% saline. Trametinib release profiles were affected by the amount of membrane coated onto the NPs, with the most sustained release from the NPs proportional with the highest amount of membrane used. The cytotoxicity result showed that membrane coated PLGA

nanoparticles were cyto-compatible in human dermal fibroblast cells up to a concentration of 1000 μg/mL. They were also hemo-compatible, with hemolysis less than 5%. In binding and cellular uptake studies, 19LF6 membrane-coated NPs displayed a significantly greater binding capacity than that of the negative controls (NPs coated with membranes from T-cells not specific to melanoma). Moreover, the binding kinetics and cellular uptake of these particles were shown to be membrane/TCR concentration dependent. Their cancer killing efficiencies were significant and aligned with binding and uptake characteristics. Particles with the higher membrane content (greater anti-gp100 TCR content) were shown to be more effective when compared to free drug and the negative controls. Based on these *in vitro* studies, these T-cell membrane cloaked NPs could potentially be used to improve the chemotherapeutic treatment of melanoma.

Table of Content

List of Illustrations

List of Tables

Chapter 1

Introduction

1.1. Background and statistics of melanoma

The skin is the largest organ of the body and serves several key functions such as protection from infection and injury and regulation of body temperature (1, 2). The skin itself has three layers: epidermis, dermis, and hypodermis (Figure 1). Melanocytes are cells of the epidermis that serve in producing the pigment melanin, which gives skin its color. Skin cancer is characterized by the uncontrollable growth of abnormal cells in a layer of the skin (3,4). It has three common forms: basal carcinoma, squamous cell carcinoma, and melanoma (5,6,7). Melanoma is one of the less common skin cancers, and despite this, it is the most malignant/metastatic skin tumor which originates from melanocytes (8,9). Melanoma is the fifth most common cancer type in the United States. The American Cancer Society estimates that in 2017, approximately 87,110 new cases (52,170 men, 34,490 women) will be diagnosed and about 9,730 individuals (6,380 men, 3,350 women) will die from the disease (2).

1.2. The risk factors and incidence

There are many risk factors associated with melanoma, including skin color, sun exposure and family history (Figure 1). The incidence of melanoma does have a large dependence on physical features like hair color, eye color, and skin color of the individual (10,11). Individuals with lighter skin appear to be more affected. Although, it can arise in any part of the body, the neck and face remain the more common sites for melanoma. The most common risk factor is ultraviolet radiation (UV) from the sun (12, 13). Other risk factors include acute sunburns, precancerous lesions, exposure to carcinogens, presence of moles on the body, family history of skin cancer, and adverse

environmental conditions.

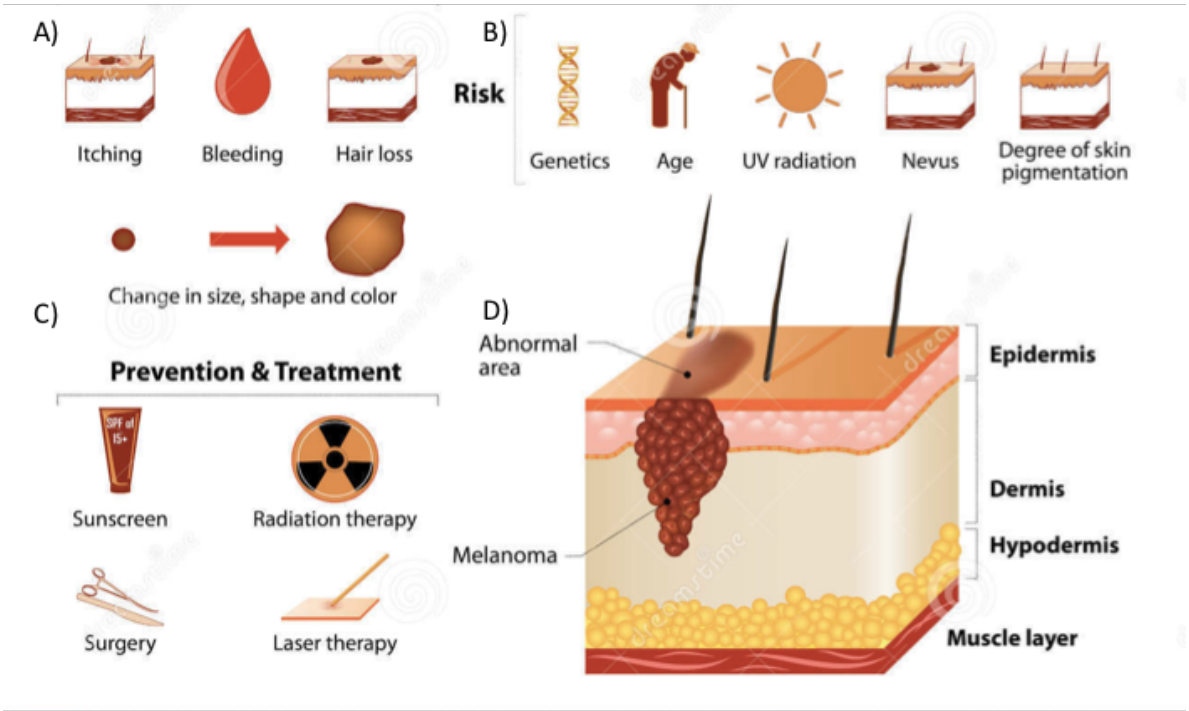

Figure 1: <u>Melanoma symptoms, risk factors and available treatments</u>: A) Signs and symptoms. B) Risk factors. C) Prevention and treatment. D) Representative anatomy [14].

1.3. Current treatment and limitation

Treatment methods are dependent on the stage of melanoma. The 5-year survival rates for patients diagnosed with early-stage melanoma are estimated to be 98% as opposed to 62% with melanoma that has spread to nearby lymph nodes. In the situations where the malignant cells have spread to other parts of the body (Figure 2), the survival is estimated to be 18% (15). Melanoma levels can be classified based on the degree of invasion. All classes have different treatment options and with different the survival rates (Table 1).

Table 1: Melanoma stages and their respective treatments (16).

Stage	Degree of Tumor Invasion	Treatment options
Level 1	Malignant melanocyte is confined to epidermis (<1 mm)	Surgery
Level II	Malignant melanocytes infiltrate papillary dermis singly or in small nests (1-2 mm)	Surgery
Level III	Malignant melanocytes fill and expand papillary dermis, with extension of tumor to papillary-reticular dermal interface (usually signifying vertical growth phase) (>2-4 mm)	Surgery, Adjuvant therapies, radiation
Level IV	Malignant melanocytes infiltrate reticular dermis in significant fashion (>4 mm)	Surgery, chemotherapy and radiation therapies
Level V	Melanoma can be any thickness, and spread to distant lymph nodes or to distant sites (e.g. lung, liver, brain, bone).	Immunotherapy, targeted therapy, chemotherapy, radiation therapy

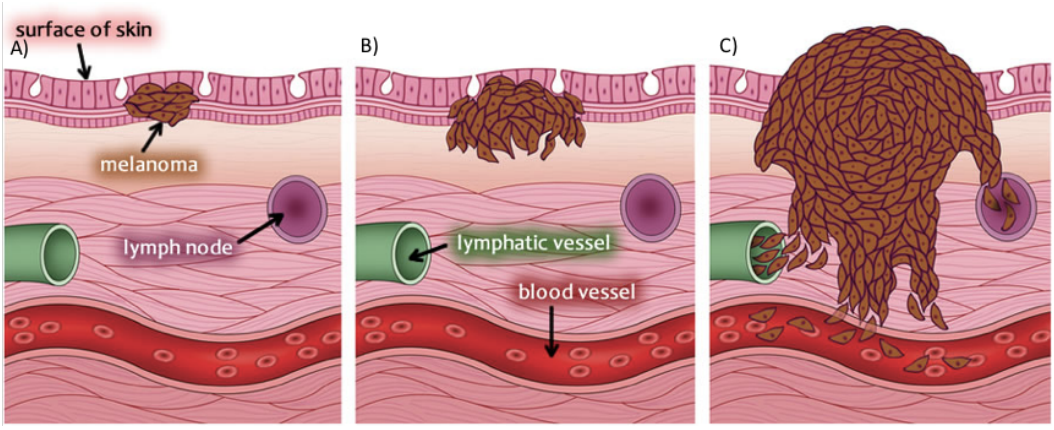

Figure 2: <u>Growth mechanism and stages of melanoma</u>: A) early stage of melanoma, B) migration of melanoma into deeper tissues and C) metastasis to other parts of the body through lymphatic and blood vessel [17].

Early stages of melanoma are often treatable with surgery; however, the tumor thickness and location are important. The acceptable size of a tumor to be effectively treated with surgery is within 0.5 cm with about a 0.2 cm margin (18). In the case of larger and more advanced melanomas, surgery is often not effective. The advantage of surgery is that tumors of acceptable size are easily removed, while avoiding the side effects of radiation and toxic chemotherapy. It is, however, important to know whether the tumor has spread to any lymph nodes. Thus, a biopsy of the regional lymph nodes should be included if surgery is elected. If a cancerous growth is found, the lymph nodes are also dissected surgically along with the tumors. However, surgery itself has a variety of complications, including long-term swelling of organs and slow recovery.

Many advances have been made for the treatment of more aggressive melanoma stages, including improved chemotherapy, targeted therapy, immunotherapy, radiotherapy, and the combinations of the two (19). Chemotherapy and targeted therapy involve the administration of drugs that often stop DNA transcription or block intracellular signaling pathways in the hope of inhibiting cell growth and replication. Radiation therapy utilizes high-energy rays to damage cellular DNA, and immunotherapy focuses on activation of one's immune cells against the cancerous cells (20). Radiation therapy is useful for shrinking tumor size and reducing the symptoms of cancer, but does not significantly treat the tumor. In chemotherapy, drugs, such as dacarbazine, cisplatin, vinblastine, and temozolomide are widely used. A novel mitogen-activated extracellular signal-regulated kinase (MEK) inhibitor, Trametinib, was approved by the US Food and Drug Administration in May 2013 as a single agent for the treatment of BRAF V600E/K mutant metastatic melanoma (21). While there are a wide number of therapies and drug combinations available for the treatment of melanoma, a key limitation in the efficacy of chemotherapy is the severe side effects and the development of multidrug resistance during prolonged treatment.

Radiotherapy or immunotherapy can often be combined with chemotherapy for a more effective outcome (5). Chemotherapy and the listed traditional treatments, however, are often accompanied with insufficient response rates and numerous severe side effects owing to the low efficacy and non-specific mechanisms of drug delivery (21).

One particular focus of interest in immunotherapy encompasses technologies such as cell therapy. Immune cells are isolated from immunosuppressed cancer patients and reprogrammed *in vitro* against cancer antigens (specific to the cancer present in the patient). Current research has mostly focused on the modification of dendritic cells and T-cells, with T-cell based cancer immunotherapy having been used effectively in cancer treatment (22). T-cells are collected from patient's own body and engineered to generate specific receptors on their surface. These receptors are referred to as chimeric antigen receptors (CARs) which are a specific type of protein located on tumor cells, and provide the T-cells with a way to recognize and kill cancer cells (23). Although these methods have been proven to be effective, they are accompanied by several limitations. Along the high costs and complexities of isolation, the long-term presence of re-programmed cells in the body poses some major concerns (23). The possible risks of long term survival of re-programmed cells have included the development of autoimmune disease and can subsequently lead to death. To overcome the limitations of current chemotherapy and immunotherapy methods, novel nano-technological advances have been introduced.

1.4. Nanoparticles in melanoma treatment

Nanoparticle-based drug delivery systems have recently been used for cancer treatments. Nanoparticles possess several advantages, including increased stability, enhanced carrier capacity, varied feasible methods of administration and the ability to incorporate both hydrophilic and

hydrophobic types of drugs (24). Nano-vehicles often serve to protect the drug and can be customized to release the drug in a sustained fashion. Sustained kinetics could lead to enhance drug bioavailability at the cancer site and reduce its toxicity to healthy tissues. Additionally, nanoparticles can be designed to deliver and monitor multiple agents simultaneously. For instance, nanoparticles have loaded with both diagnostic and therapeutic capabilities reagents for theranostic applications. In these applications, imaging and treatment can be monitored at the same time (25). Several currently studied, nano-based drug delivery platforms for melanoma include liposomes, dendrimers, polymersomes, carbon-based nanoparticles, and protein-based nanoparticles (26). Polymerosomes are widely studied due to their long-term stability and ability to provide a sustained drug release over prolonged periods of time. Current FDA approved examples of polymers include PLGA (polylactic-co-glycolic acid) and PLA (polylactic acid). Even though such polymers are considered to be biocompatible, they are still far from complete immune evasion (27). Numerous modifications have been studied over the last few decades in the hopes of giving polymeric nano-carriers the ability to escape the immune surveillance. Several of these modifications include PEGylation, plasma-surface modification and lipid-based masking (Table 2). Of those lipid masking has raised an interest due to the ability of lipids to provide better "stealth" properties for foreign biomaterial-based vehicles to remain unnoticed in the face of immune cells.

1.5. Biomimetic nanoparticles in cancer treatments

Several of the stealth functionalities of synthetic and biopolymers are used to enable prolonged pharmacokinetics and improve bio-distribution of the particles. Table 2 provides some of the current strategies for use in nano-carriers used in cancer treatments.

Table 2: Current nano-carriers in cancer treatments (26).

Strategy	Advantages	Disadvantages
Sustained-release		
Zinc-complex	Easily performed; can be adopted in other studies	Limited improvement on prolonging release time
Microsphere[78]	Easily prepared; commercially available for many materials	Acidic degradation of PLGA denaturation of rhGH
Hydrogel	Long and adjustable sustained-release; easily prepared	Adverse effect at injection site; shorter sustained-release time than microspheres
Prolonged half-life		
PEGylation	Reduced clearance; adjustable half-life based on PEGylated site	Initial burst (some studies have addressed this); storage problem in the solution state
Albumin conjugation	13–15 h half-life in monkeys	Possible adverse event such as lipoatrophy; feasibility of scale-up
XTEN amino sequence fusion	110 h half-life in monkeys	May alter the potency of rhGH
Hybrid Fc fusion	High bioavailability	
Carboxy-terminal peptide fusion	No adverse effect observed 1 month efficacy in human B lymphocytes	Low bioavailability
Extracellular receptor of hGH fusion	1 week efficacy has been demonstrated in a Phase II trial; 10 d effect in rats	Further study in animal model required

The biomembrane-coated nanoparticles present a comprehensive evasion strategy against the multi-faceted nature of immune clearance. Cell membrane coated biomimetic nanoparticles have made an impressive contribution to the improvement of cancer therapy (28). Due to cell membrane structure and retained cellular antigens, biomimetic NPs carry special advantages, such as long blood circulation, ligand recognition, immune escape, homotypic targeting, and the ability for a sustained drug delivery (29). Recently, cell membrane coated nano-systems with unique features and functions have been created by coating synthetic nanoparticles with cell membranes isolated from different cell types, such as red blood cells, platelets, and leukocytes. *Parodi et al.* (30) created leukocyte-membrane-cloaked silica micro particles which possessed endothelium-traversing properties, and these particles achieved receptor ligand interaction and enhanced their circulation time. Studies performed by *Hu et al*. (31) focused on creating platelet membrane-coated nano-vehicles with cancer targeting capabilities. *Frank et al*. (28) reported that cancer cell

membrane-coated nanoparticles were suitable for homotypic cancer targeting and effective cancer immunotherapy.

1.6.Overview of research project

The overall goal of this project is to develop hybridoma T-cell membrane-coated PLGA nanoparticles (T-MNPs) for targeted chemotherapeutic treatment of melanoma (Figure 3). Melanoma cells carry various biomarkers, including gp100 antigen (32). The 19LF6 hybridoma T-cell line was genetically engineered to express and present anti-gp100 antigen T-cell receptor (TCR). In this project, a 19LF6 membrane was used for coating PLGA NPs in the hopes of establishing a targeted chemotherapeutic drug delivery platform to gp100-presenting melanoma cell lines, such as 1520 and DM-6. Mechanism of TCR interaction with tumor-specific antigens is represented in Figure 4. A549 (lung cancer line) and DO11.10 (T-cell line; non-specific to gp100) membrane coated PLGA NPs were also formulated (A-MNPs and D-MNPs, respectively). These particles were used as negative controls due to their lack of specificity to gp100 antigens.

Overall, three types of membrane-coated NPs were created, as shown below:

- 19LF6 cell line (T-cell) coated NPs (T-MNPs) – positive control
- DO11.10 cell line (T-cell) coated NPs (D-MNPs) – negative control
- A549 cell line (lung cancer) coated NPs (A-MNPs) – negative control

PLGA polymer was chosen due to its below advantages:

- Bio-compatibility and bio-degradability (24)
- FDA and European Medicine Agency approval (24)
- Adaptability to hydrophobic and hydrophilic drugs (24)
- Sustained drug release kinetics (24)

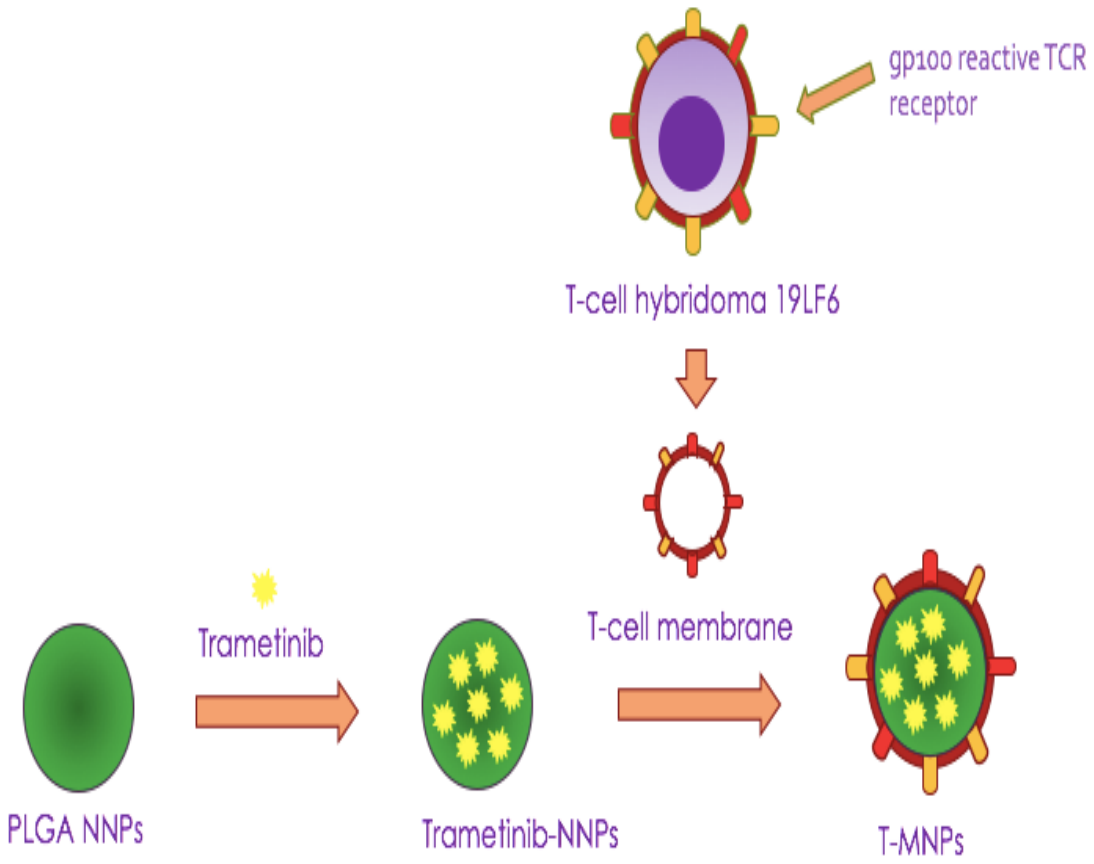

Figure 3: Design of membrane coated nanoparticles (MNPs)

Chemotherapeutic drug Trametinib was selected due to its effectiveness against cancer cell lines carrying a V600E BRAF oncogenic mutation such as DM-6 and 1520 cell lines (33). Trametinib is an FDA approved MEK (MEK 1 and 2) that can also be used in combination with other approved anti-melanoma drugs, such as drafatenib. Specific cell signaling mechanism affected by Trametinib is represented in Figure 5.

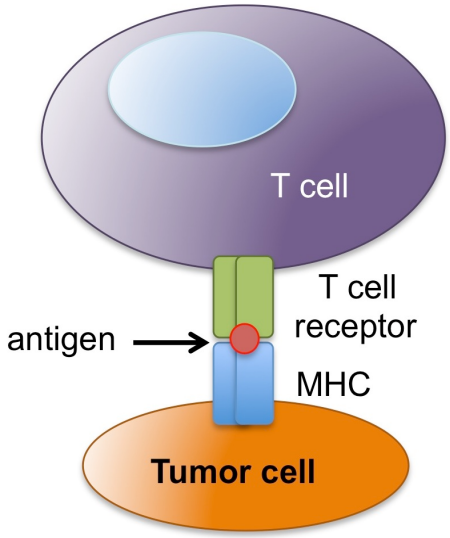

Figure 4: Mechanism of tumor cell recognition by tumor specific TCR [33].

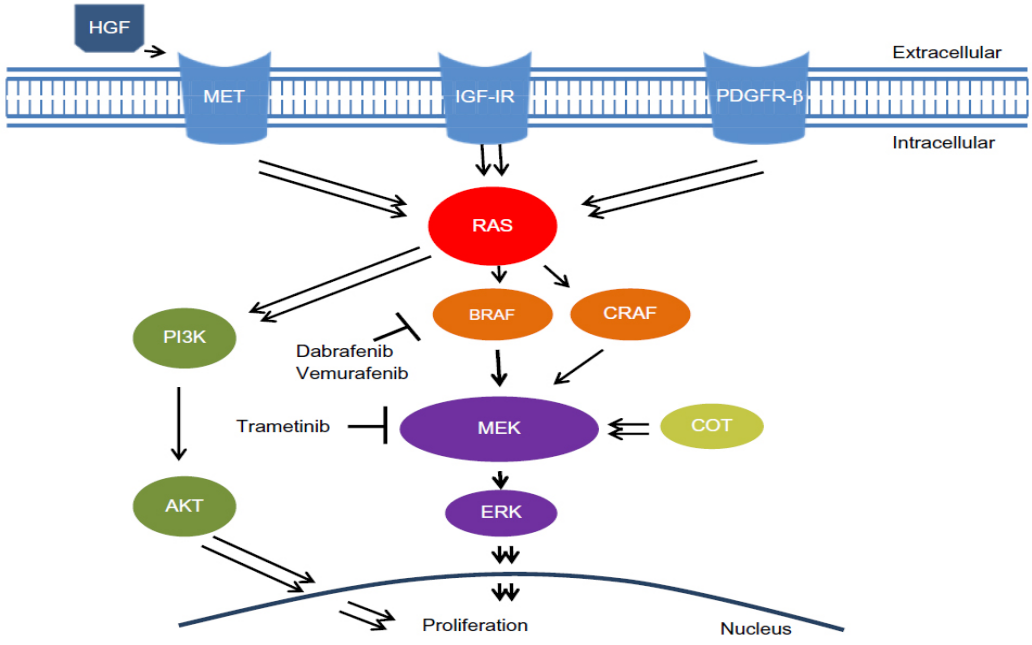

Figure 5: Cell signaling mechanism associated with Trametinib. MEK shown here as a downstream target of BRAF [34].

It was hypothesized that the presence of anti-gp100 TCR on T-MNPs would specifically target gp100 presenting melanoma cells and enhance cellular uptake of T-MNPs. Proposed uptake kinetics and T-MNP effect on cancer cells are illustrated in Figure 6. Chemotherapeutic drug Trametinib is predicted to inhibit MEK activity in b-RAF mutate melanoma cells and inhibit cell survival and proliferation. Therapeutic efficiency of T-MNPs was predicted to be significantly enhanced when compared to that of non-specific membrane coated (A-MNPs and D-MNPs) and naked PLGA NP.

Three specific aims to test on hypothesis and to reach our goals are:

Aim 1 - Develop membrane coated MNPs

- ❖ Synthesis of naked PLGA NPs (NNPs)
- ❖ Extraction of 19LF6, DO11.10 and A549 cellular membranes
- ❖ Extrusion of PLGA NPs with cellular membranes

Aim 2 – Characterize T-MNPs

- ❖ Determine MNP size and morphology
- ❖ Examine the functionality and binding efficiency of TCR in T-MNPs
- ❖ Validate TCR presence on T-MNPs

Aim 3 - Investigate targeting capability and therapeutic efficiency of T-MNPs *in vitro.*

- ❖ Evaluate melanoma cell uptake of T-MNPs in comparison to that of non-specific MNPs
- ❖ Test the therapeutic efficiency of T-MNPs in comparison to non-specific MNPs
- ❖ Determine MNP cyto- and hemo-compatibilities of T-MNPs

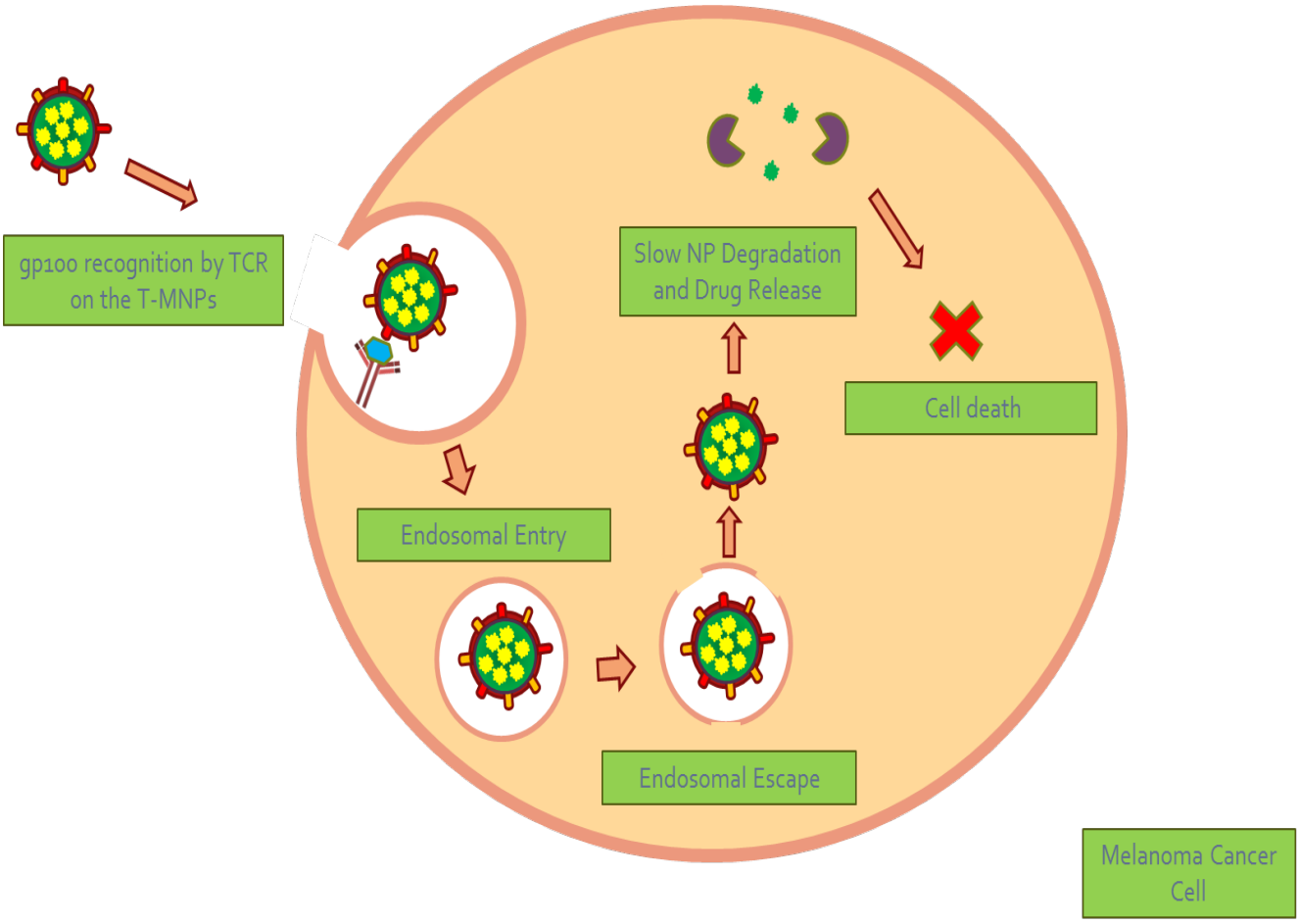

Figure 6: Proposed uptake and therapeutic mechanisms of T-MNPs

The novelty of this project encompasses the development of cell membrane-coated NPs that are able to retain high integrity and functionality of cell receptors such as TCR. These particles are predicted to be superior due to the incorporation of T-cell membranes consisting of anti-cancer TCR. A successful outcome of this project could avoid the necessity and complexity of cell therapy techniques as described above.

CHAPTER 2: Material and methods

Experimental Methods

2.1. Materials

Poly (D, L lactide-co-glycolide) (PLGA) (inherent viscosity 50:50 with carboxyl end groups) was purchased from Akina (PolySciTech, West Lafayette, IN). Poly (vinyl alcohol) (PVA, mw 30,000-70,000) and DCM (Dichloromethane) were obtained from Sigma Aldrich (MO, USA). Trametinib, coumarin-6, Tris-HCL, D-glucose, B-Mercaptoethanol, Phenylmethylsulfonyl fluoride (PMSF), Protease inhibitor cocktail, Triton® X-100, Dimethyl sulfoxide (DMSO) and RPMI-1640 were received from Sigma Aldrich. The Avanti Polar Lipids Mini Extruder Kit was gotten from Avanti Polar Lipids. RIPA buffer was purchased from Alfa Aesar. SDS-PAGE gel, and Mini PVDF transfer pack were received from Bio-rad. TCR β chain (Armenia Hamster IgG) - antibody and its isotype antibody were bought from BD Biosciences. NuetrAvidin biotin binding protein, Superblock solution, BCA assay kit and DNAse were obtained from Thermofisher Scientific. Foamvar coated-copper TEM grids were purchased from Electron Microscopy Sciences. Fetal bovine serum (FBS), 1X trypsin EDTA, Dulbecco's Modified Eagle's Medium (DMEM) and penicillin-streptomycin were received from Invitrogen.

Biotinylated gp100-HLA-A2/B2M (gp100 refold) and biotinylated GIGL peptide-HLA-A*201/B2M complexes were synthesized and contributed by Dr. Jon Weidanz's laboratory. gp100 refold: heavy chain and Beta2Microglobulin chain were expressed in and harvested from E. coli in the form of inclusion bodies. The complex was biotinylated using Avidin Biotinylation kit [Bulk BirA: BirA biotin-protein ligase bulk reaction kit]. g100-2M (209-217) peptide was purchased from Genscript. bGIGL complex was synthesized in a similar fashion. 19LF6, DO11.10, DM-6,

and 1520 cell lines were obtained from Dr. Jon Weidanz's lab.

2.2. Synthesis of PLGA nanoparticles

PLGA nanoparticles (naked NPs; NNP) were synthesized via a standard single emulsion (O/W) technique. Briefly, 90 mg of PLGA 50:50 and 4.5 mg of Trametinib were dissolved in 3 mL of DCM and sonicated at 30 W for 2 minutes to allow dispersion of PLGA and Trametinib in the solvent. The resulting solution was added in a dropwise to 15 mL of filtered 5% (w/v) PVA under stirring conditions. The suspension was then sonicated at 30 W for 10 minutes (1 min ON, 30 sec. OFF). The solution was allowed stirring overnight to evaporate the organic solvent. After 24 hours, the obtained nanoparticle solution was centrifuged at 15,000 rpm for 30 minutes. The supernatant was saved for drug loading evaluations and the PLGA NP pellet was re-suspended in 3 mL of DI water followed by freeze-drying for 24 hours. PLGA NPs loaded with coumarin-6 for cellular uptake studies were performed using similar procedure.

2.3. Cell lines and culture conditions

DM-6, 1520, A549 and 19LF6 cell lines were maintained in RPMI-1640, supplemented with 10% (v/v) fetal bovine serum (FBS) and 1% (v/v) penicillin streptomycin. DO11.10 and HDF cell lines were maintained in high glucose DMEM, supplemented as described for RPMI-1640. All cells were incubated at 37˚C, 5% CO_2.

2.4. Cell membrane extraction

To harvest the cell membrane, cells were first grown to confluency in T-225 cell culture flasks. Cells were isolated by trypsinization and centrifuged at 1000 rpm for 5 minutes. To remove any remaining media contents, the cells were washed with cold 1X PBS and centrifuged at 1000 g for 10 minutes. The resulting pellet was re-suspended in hypotonic lysis buffer (10 mM Tris-HCL, pH= 7.5) supplemented with the ready-to-use protease inhibitor cocktail. The solution was kept on ice for 20 minutes and then centrifuged at 1000 g for 10 minutes. The pellet was re-suspended in cold 0.25 X PBS and kept on ice for 20 minutes followed by centrifugation at 800 g for 5 minutes. The final pellet was collected in cold 1X PBS. The cell membrane mix was analyzed for the DNA and protein content using Nano-Drop 1000 Spectrophotometer (Thermofisher Scientific) and BCA assay kits, respectively. To eliminate any remaining DNA contents, DNAse reaction was performed on the cell extract (amount of DNAse added varied with DNA content) by incubation with DNAase for least one hour at 37°C.

2.5. Preparation of membrane coated NPs (MNPs)

Poly (lactic-co-glycolic acid) (PLGA) nanoparticles (naked NPs; NNPs) were coated with various cell membranes (MNPs). These particles were loaded with an FDA-approved chemotherapeutic drug Trametinib, suitable for treatment of melanoma cell lines containing V600E BRAF mutation. Briefly, NNPs were re-suspended in cell membrane solution at different NNP weight to membrane protein weight ratios (w/w): 1:0.5, 1:1, 1:2 and 1:3. The mixture was then extruded 22 times using a pre-heated Avanti Polar Lipids Mini Extruder (37°C). The extrusion was performed using a 200-nm polycarbonate membrane. The resulting membrane coated NPs (MNPs) were dialyzed with a

100 kDa MWCO dialysis membrane for 2 hours. Prior to freeze-drying, dialyzed MNP solution was supplemented with D-glucose at a final concentration of 1mg/mL.

Three types of membrane-coated NPs were created. As shown below:

- 19LF6 cell line (T-cell) coated NPs (T-MNPs) – positive control
- DO11.10 cell line (T-cell) coated NPs (D-MNPs) – negative control
- A549 cell line (lung cancer) coated NPs (A-MNPs) – negative control

2.6. Characterization of MNPs

2.6.1. Particle size, zeta potential, and morphology

Nanoparticle size, polydispersity index, and zeta potential were measured using Dynamic Light Scattering (DLS). Briefly, to measure the size of NNPs, NNP suspension (10 μL of 500 μg/mL) was added to 3 mL of deionized water and inserted into the DLS in a compatible cuvette. MNPs sample was prepared in a similar fashion, but in 1X PBS (pH 7.4). To generate TEM images of MNPs, 10 μL of 250 μg/mL MNP suspension was added to plasma-treated Formavar Square Mesh Copper Grids for 20 mins. Then suspension 10 μL of 0.5% uranyl acetate solution was applied onto the same grid for 20 min. The uranyl acetate solution was removed and the grid was dried overnight in a vacuum desiccator.

2.6.2. Identification of TCR in T-MNPs

Flow cytometric staining was used to identify anti-gp100 T-cell receptor (TCR) on T-MNPs. First, the particles were stained with TCR- β chain to evaluate the presence of any TCR or TCR components on synthesized MNPs. Briefly, 1mg/mL of MNP solution was prepared in staining buffer (0.5 % BSA, 1mM EDTA in 1X PBS). Then 200 μL of the solutions were aliquoted into 3

separate tubes for “stained”, “unstained” and “isotype control” groups. “Stained” and “isotype control” groups were mixed with Armenia Hamster anti-TCR$^{\beta}$ and Armenia Hamster IgG antibodies at 1:100 dilution, respectively. “Unstained” group contained MNPs and NNPs in staining buffer only. The solutions were vortexed, incubated for 30 minutes, and protected from light. The samples were then washed with the staining buffer 3 times and centrifuged at 14,000 rpm for 20 minutes each time. Each of the groups was then analyzed using a BD Biosciences FACS Diva Flow cytometer.

After validation of TCR- β chain presence, 1 mg/mL of MNP solution was aliquoted into 2 separate tubes for “stained” and “unstained” groups. “Stained” group was mixed with a custom-made APC-gp100/HLA-A2 complex (described in section 2.1) at 1:100 dilution. “Unstained” group only contained MNPs staining buffer. The solutions were vortexed, incubated for 30 minutes, and protected from light. The samples were then washed with the staining buffer 3 times and centrifuged at 14,000 rpm for 20 minutes each time. Each of the groups was then analyzed using a BD Biosciences FACS Diva Flow cytometer. 10,000 events were collected per sample, gated and reference by unstained NPs. Histograms were plotted with fluorescence intensity on the x-axis using a biexponential scale.

2.6.3. Binding kinetics of MNPs

The binding characteristics of T-MNPs were studied using ResoSens label-free optical detection. In this study, T-MNPs with highest and lowest NP weight to membrane weight ratios, 1:0.5 and 1:2, were chosen. These nanoparticles were then tested at varying concentrations. D-MNPs were tested at the highest NP to membrane protein ratio (w/w) (1:2) and at a concentration 2-fold higher

than the highest concentration used for T-MNPs. All samples were tested against specific gp100-refold and non-specific refold bGIGL (described in 2.1. section).

2.6.4. T-MNP stability studies

Stability of T-MNPs with varying NP weight to membrane protein weight ratios (w/w) was evaluated by monitoring particle size at pre-determined time-points using Dynamic Light Scattering. To observe the stability of T-MNPs, particles of different ratios were incubated in 0.9% saline over 48 hrs. T-MNP solutions were prepared as described in section 2.6.1, and the size of particles was measured at pre-determined time points (0, 0.5, 1, 3, 6, 12, 24, and 48 hours).

2.6.5. Drug loading and drug release kinetics of T-MNPs

The supernatant collected in the nanoparticle synthesis was used to determine the drug loading efficiency by an indirect method. The Trametinib loading efficiency was calculated using the following formula:

$$\%\ \text{Loading Efficiency} = \frac{\text{amount of drug used} - \text{amount of drug in supernatant}}{\text{amount of drug used}} \text{x}100$$

The drug release study was carried out for a period of 28 days. Briefly, 1 mg of NNPs and T-MNPs (NP: membrane protein weight (w/w) ratios of 1:0.5, 1:1 and 1:2) were measured. Each of the samples (1mg/mL) was incubated at 37°C. At each pre-determined time-point, the samples were centrifuged at 14000 rpm for 30 minutes, and supernatants were collected and stored at -20 °C for later analysis. The pellets were re-suspended in fresh 1X PBS and incubated for further time points. Each of the drug release aliquots was analyzed using a UV-vis Spectrophotometer at 330 nm. The amount of drug released was determined against a standard curve for Trametinib.

2.7. *In vitro* studies of T-MNPs

2.7.1. SDS-PAGE protein analysis and Western blotting

Three cell lines were used to analyze gp100 protein content: A549,1520, and DM-6. Cells were first washed with 1X PBS and isolated by trypsinization. The cell suspensions were then centrifuged at 1000 rpm for 5 minutes. The cell pellet was re-suspended in 1X PBS and centrifuged at 1000 rpm for 5 minutes. 2 million cells were re-suspended in 200 µl of 1X RIPA buffer with 1 mM PMSF and incubated for 20 minutes on ice. The solution was centrifuged for 20 minutes at 14000 rpm at 4°C. Supernatant was collected and a BCA assay was performed to determine the protein concentration. 4X Laemeili buffer with Beta-Mercaptoethanol were used to prepare 10% final concentration buffer. 8 µg of protein was mixed with 7.5 µL of 4X Laemeili Buffer/Beta-Mercaptoethanol, 2 µL of protein solution and 20.5 µL of Proteinase-free water. The sample was heated at 90°C for 10 minutes. The samples were quickly centrifuged to bring down the condensation and cooled to room temperature. 20 µL of the samples was applied into a ready-to-use SDS-PAGE gel. The electrophoresis assembly was connected to a power supply set at 150 V, 400 mA and the samples were run for about 30 minutes or until the dye reached to the bottom of the gel. The gel was placed into a ready-to-use Mini PVDF transfer pack. The experiment was run about 7 minutes for 2 gels using Trans® Turbo™ Transfer System. After protein transfer, blotted membrane was placed into a small container containing 5% BSA/TBST (1X .05% Tween/Tris-buffered Saline) blocking solution. The membrane protein was placed side up for 1.5 hours at room temperature. Blocking the membrane prevents non-specific background binding of the primary and/or secondary antibodies to the membrane. Primary antibody against gp100 was prepared in 2.5 % BSA in TBST and the membrane was incubated with primary antibody for overnight at 4°C

with shaking. The membrane was washed 3 times thoroughly with adequate volume of TBST solution to remove any unbound, excess antibody. The unconjugated primary anti-body was incubated with a conjugated secondary anti-body in 2.5% BSA/TBST for 1-2 hours and washed 3 times with TBST. The membrane was also blotted with β-actin and served as a control. The blotted membrane was imaged using ChemidocTM Imaging System.

2.7.2. Real-time PCR

Melanoma cell lines DM-6 and 1520 and A549 human lung carcinoma cells were used. Cells were detached by trypsinization and centrifuged at 500 g for 5 minutes. Total RNA was isolated from cell pellets by using an RNeasy Plus Mini kit according to the manufacturer's instruction. To reduce contaminating genomic DNA from RNA, proper RNA isolation and cDNA synthesis procedures were followed. cDNA synthesis was performed using High-Capacity cDNA Reverse Transcription Kit by T100^{TM} Thermal Cycler. The cDNA reaction was run using the following setting in sequence:

1. 25°C for 10 min
2. 37°C for 2 hrs.
3. 85°C for 5 min
4. 4°C at ∞

After the reaction was competed the samples were prepared by the following mix: 2.5 μL of sample, 12.5 μL of PowerUp^{TM} SYBR^{TM} Green Master, 8 μL of Nuclease-free water, 1μL of sense primer, and 1μL of anti-sense primer. PCR reaction was run using the following setting in sequence:

1. 96°C for 1 min
2. 96°C for 15 sec.
3. 57°C for 30 sec.
4. 68°C for 1 min
5. 32 X go to step 2
6. 68°C for 10 min
7. 12°C for ∞

2.7.3. Cellular uptake of T-MNPs

To determine cellular uptake of nanoparticles, 1520 (gp100 positive), DM-6 (gp100 positive) and A549 (gp100 negative) cell lines were seeded and allowed to grow for 24 hours. Coumarin-6 (C-6; fluorescent dye) loaded T-MNPs (gp100 refold specific) and D-MNPs (non-specific to gp100 refold) at varying NP to membrane weight ratios: 1:0.5, 1:1 and 1:2, were utilized for the uptake study. Cells grown in media without nanoparticles served as a negative control. To study cellular uptake of MNPs, serially diluted MNP concentrations (100 µg/mL, 250 µg/mL, 500 µg/mL, 1000 µg/mL) at different NP to membrane ratios were prepared. The cells were exposed to different MNPs groups for approximately 2 hours, subsequently washed with 1X PBS and lysed with 250 µl/well of 1% Triton® X-100 (approximately 30 min incubation). Cell lysis extracts were then analyzed for the protein content using the Pierce BCA protein assay kit (Thermo Scientific, Rockford, IL) and C-6 fluorescent intensity (emitted from particles uptaken inside the cell) using a UV-vis Spectrophotometer (458/540 em/ex). Total protein concentration in each lysate was determined using a BSA standard curve. The uptake of the nanoparticles was calculated by normalizing the particle concentration (determined from fluorescence intensity in a lysate) in each sample with total cell protein, which correlated to the number of cells in the sample.

2.7.4. Pharmacokinetic and therapeutic study

The cells used in this study were melanoma DM-6 and 1520 cell lines. Firstly, the cells were exposed to free drug in known concentrations (1.2, 2.5, 5, 10, 15, 20, 25, 50, 75, and 100 μg/mL) for a period of 72 hours to determine the IC50 value of Trametinib. After IC50 values were obtained in both cell lines, the therapeutic study was performed. Therapeutic efficiency was tested with 1:2 NP weight to membrane weight ratio T-MNPs (specific), A-MNPs (non-specific), and D-MNPs (non-specific) as well as free drug and NNPs. Three different NP concentrations (0.83 μg/mL, 1.66 μg/mL, and 2.5 μg/mL for DM-6; 15 μg/mL, 29 μg/mL, 44 μg/mL for 1520) were used. The cells were exposed to the described groups over 72 hrs. After 72 hours of incubation, the cell death was analyzed using MTS assays.

2.8. Safety of T-MNPs

2.8.1. Cyto-compatibility study

Cyto-compatibility study was performed on human dermal fibroblast cells (HDF). Upon reaching 80-90% cell confluency, T-MNPs and NNPs were re-suspended in media, added to cells at various concentrations (50, 100, 250, 500, and 1000 μg/mL) and incubated for 24 hours at 37°C. At the end of the incubation time, the nanoparticle suspensions were removed, and the cells were washed twice with 1X PBS. Cell viability was evaluated using MTS assays. Cells not exposed to any nanoparticles and the cells treated with 1% Triton® X-100 served as control samples, positive and negative, respectively.

2.8.2. Hemolysis and blood clotting studies

Blood clotting and hemolysis T-MNPs were evaluated using fresh human blood. Briefly, for hemolysis, 200 μL of blood was added into either 10 mL of 0.9% saline as a positive control or 10

ml of DI water as a negative control. Stock suspensions of T-MNPs were prepared in 0.9% saline at varying concentrations (50 μg/mL, 100 μg/mL, 250 μg/mL, 500 μg/mL, and 1000 μg/mL). The T-MNPs suspension (10 μL) was added into 1.5 mL centrifuge tubes. Then, 200 μL of saline diluted blood was placed into T-MNPs, saline and water samples. The tubes were incubated at 37˚C for 2 hours under gentle agitation and then were centrifuged at 1000 g for 10 minute. The absorbance of sample supernatants was monitored at 545 nm using a UV-vis Spectrophotometer.

For the blood clotting assay, T-MNP stock suspensions were prepared in 0.9% saline at different concentrations (50 μg/mL, 100 μg/mL, 250 μg/mL, 500 μg/mL, and 1000 μg/mL). T-MNPs at each concentration (10 μL) was added into 1.5 mL centrifuge tubes. Similarly, 0.9% saline and water samples were prepared as control groups. 0.85 mL of $CaCI_2$ (0.1M) was added into 8.5 mL of ACD blood to activate the blood clotting. Immediately after activating the blood, 50 μL of the blood was added to all samples. At a pre-determined time-points (10, 20, 30, and 60 min), 1.5 mL of DI water was added to all samples to inactivate blood clotting, and the samples were incubated for 5 minutes at room temperature. Supernatants were collected and monitored at 540 nm using a UV-vis Spectrophotometer.

2.9. Statistical analysis

All results were expressed as mean ± SD performed with n=3. Results obtained were analyzed using one way ANOVA with $p < 0.05$ and the student's t-test was used to identify differences between groups. $P < 0.05$ was considered to be statistically significant.

CHAPTER-3

RESULTS AND DISCUSSION

3.1. Results

3.1.1. Particle size, zeta potential, and morphology

The size of 1:2 NP to membrane ratio of T-MNPs was found to be 193±56 nm with the polydispersity of 0.265 nm size of naked NPs (NNPs) was 171.7±76 nm with polydispersity of 0.109**.** The size of membrane alone was 590.4±29 nm. The particles size was confirmed with Transmission Electron Microscopy (Figure 7A). Furthermore, TEM images of T-MNPs displayed a layer-by-layer structure for T-MNPs.

3.1.2. Identification of TCR in T-MNPs

First the presence of TCR β chain was evaluated (Figure 8A). TCR β chain stain showed a significant shift in mean fluorescent intensity 88.9 of T-MNPs when compared to that of the isotype and unstained controls (25; 27, respectively). Such result confirmed the presence of the TCR β chain component in the T-MNP formulation. The presence of a specific, anti-gp100 TCR receptor was also evaluated. The 1:2 NP weight to membrane protein weight T-MNPs were stained with APC- gp100/HLA-A2 complex (described in 2.1. section). T-MNPs showed a significant shift in fluorescence (Mean fluorescence intensity 4268 OD) when compared to the unstained control (mean fluorescence intensity 283 OD), confirming the presence a specific anti-gp100 TCR in T-MNPs (Figure 8B).

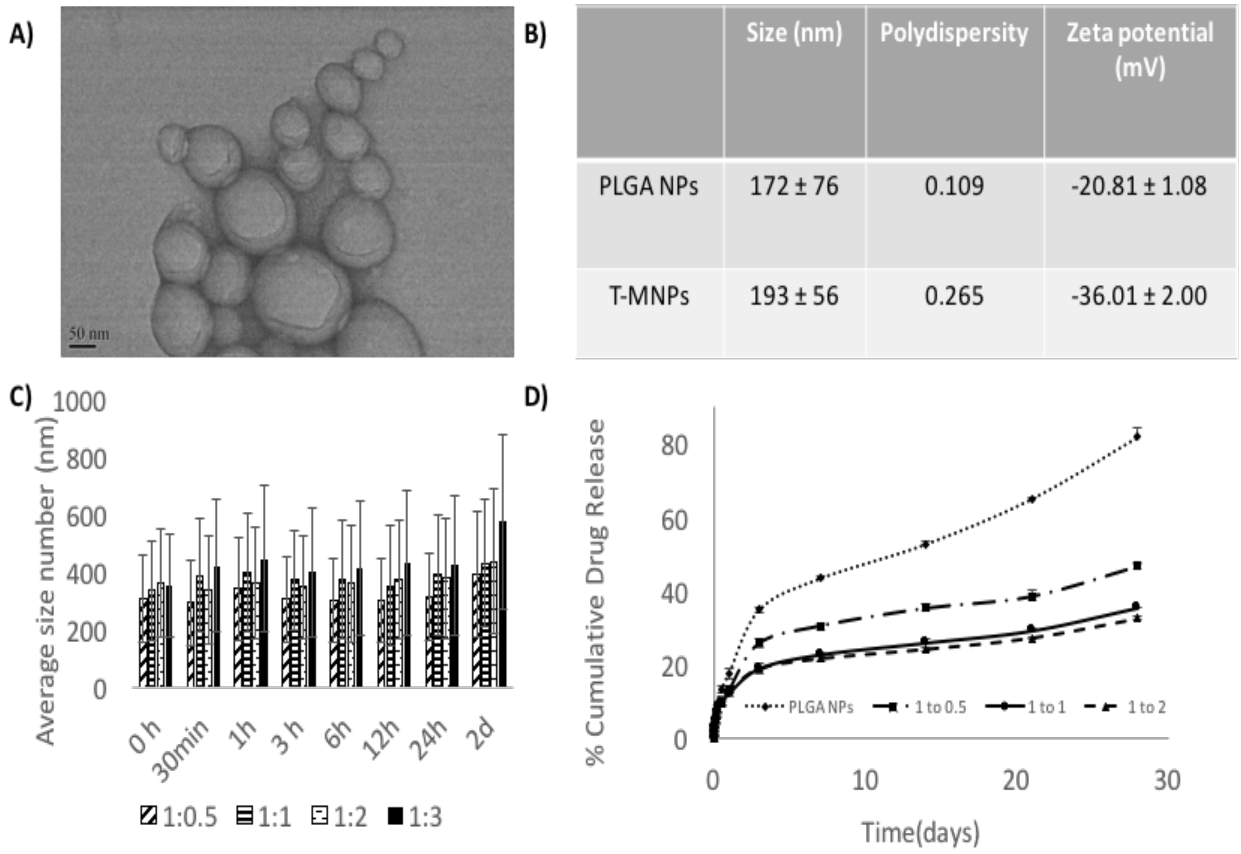

	Size (nm)	Polydispersity	Zeta potential (mV)
PLGA NPs	172 ± 76	0.109	-20.81 ± 1.08
T-MNPs	193 ± 56	0.265	-36.01 ± 2.00

Figure 7: <u>Characterization of T-MNPs</u>. A) TEM images of T-MNPs at 1:2 NP to membrane protein weight ratio. **B)** Size, polydispersity and zeta potential of PLGA NPs and T-MNPs analyzed using Dynamic Light Scattering (DLS). **C)** Stability of T-MNPs in 0.9% saline (at varying NP to membrane protein weight ratios: 1:0.5, 1:1, 1:2, and 1:3) evaluated by change in NPs size over a 2-day period using DLS. **D)** Cumulative % drug release from T-MNPs (varying NP to membrane protein ratios of 1:0.5, 1:1, 1:2 versus PLGA NPs) performed in phosphate buffered saline over 28 days. Samples were analyzed using UV-vis spectrophotometer (n=3).

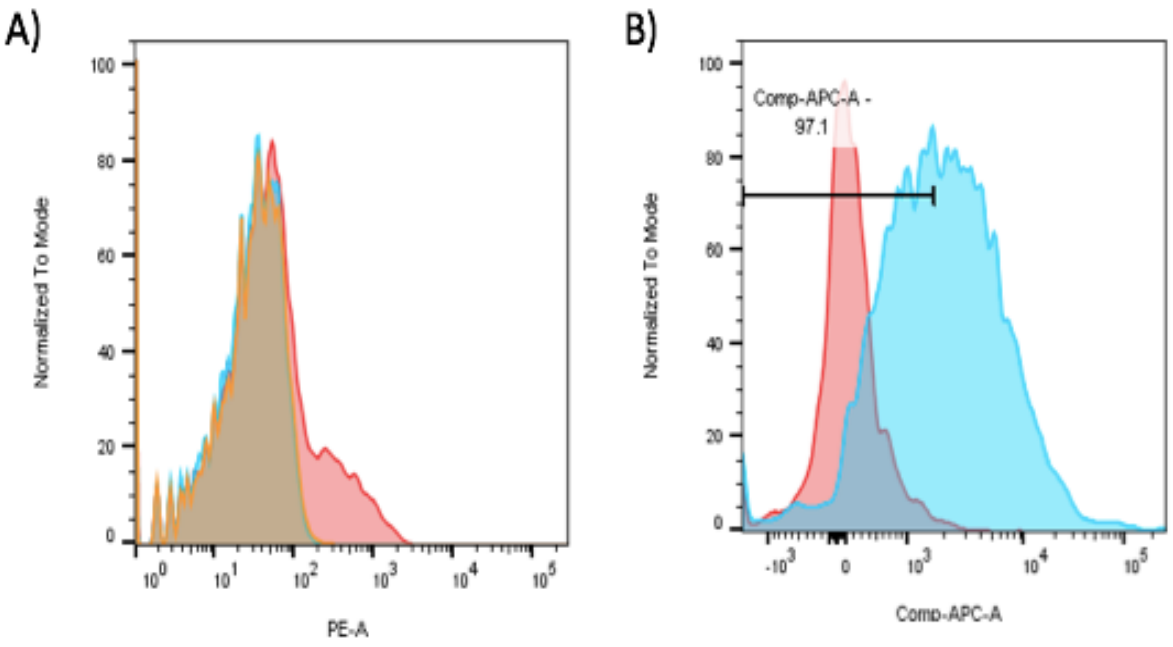

Figure 8: <u>Validation of TCR on T-MNPs</u>: A) Histogram curves demonstrated that T-MNPs expressed the TCR β chain (stained, unstained, isotype groups are represented as red, blue, orange curves, respectively). **B)** T-MNPs also consisted of APC-gp100/HLA-A2 complex (stained and unstained groups are represented as red and blue curves, respectively).

3.1.3. Binding kinetics of MNPs

As shown in Figure 9, T-MNPs bound onto gp100 as dose-dependent manner with higher binding strength observed in samples with higher concentration and higher ratio. In addition, T-MNPs at concentrations 500 µg/mL and 250 µg/mL were significantly higher when compared to the binding kinetics of 1:2 D-MNPs at 1000 µg/mL concentration.

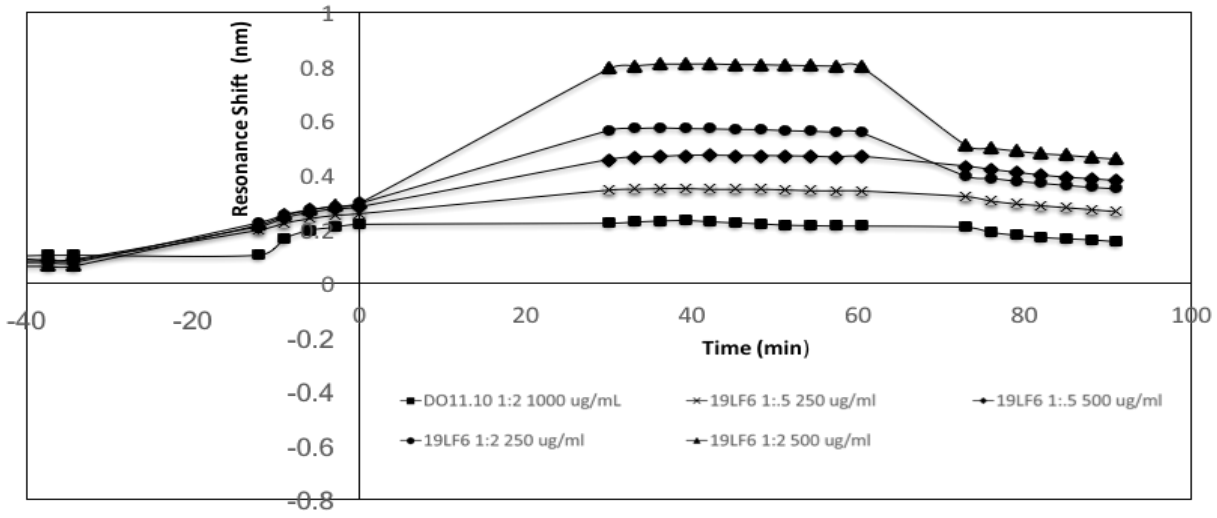

Figure 9: **Binding kinetics of MNPs:** Binding kinetics of D-MNPs (negative control), T-MNPs (positive control) and NNPs (negative control) at varying concentrations and NP to membrane protein (w/w) ratios; Kinetics were measured in terms of resonance shift over a period of time using ResoSens label-free optical detection. (n=3)

3.1.4. Stability studies of T-MNPs

The size of particles was monitored at predetermined time-points throughout the 48 hrs. Statistically, all the ratios examined (1:0.5, 1:1, 1:2 and 1:3) showed similar stability characteristics over the incubation period. The particles did not display a significant increase in size and, therefore, there was no sign of significant aggregation (Figure 7C).

3.1.5. Drug loading and drug release kinetics of T-MNPs

Drug loading efficiency of Trametinib from PLGA NPs was calculated by using the equation in section "Drug loading and drug release kinetics of T-MNPs". Loading efficiency was found to be 61%. To analyze how different membrane coating ratios would affect Trametinib release from T-MNPs, the drug release kinetics of T-MNPs with different NP: membrane weight ratios (1:0.5, 1:1

and 1:2) and naked NPs were evaluated over 21 days. Trametinib release rate was significantly slower for all ratios of T-MNPs when compared to MNPs, with lowest rate of release for 1:2 T-MNPs (Figure 7D).

3.1.6. Western blot and real time PCR

To verify gp100 expression profiles in DM-6, 1520, and A549 cell lines, western blot and RT-PCR experiments were performed. Both techniques used β-actin as a control (42 kDa, 157 bp). In Western blotting, 2 concentrations of protein lysates were tested for each cell lines: 6 ug and 12 ug (right to left, Figure 10) DM-6 and 1520 cell lines showed a significant composition of the gp100 protein (70 kDa). The relative quantity of protein in the DM-6 cell line was found to be approximately 2-fold higher than that expressed in the 1520 cell line. While, A549 showed no apparent gp100 protein composition. RT-PCR identified gp100 gene expression (751 bp) in all 3 cell lines. However, A549 expression of the gene was very low (approximately 4-fold lower) compared to those of DM-6 and 1520 cell lines. (Figure 10).

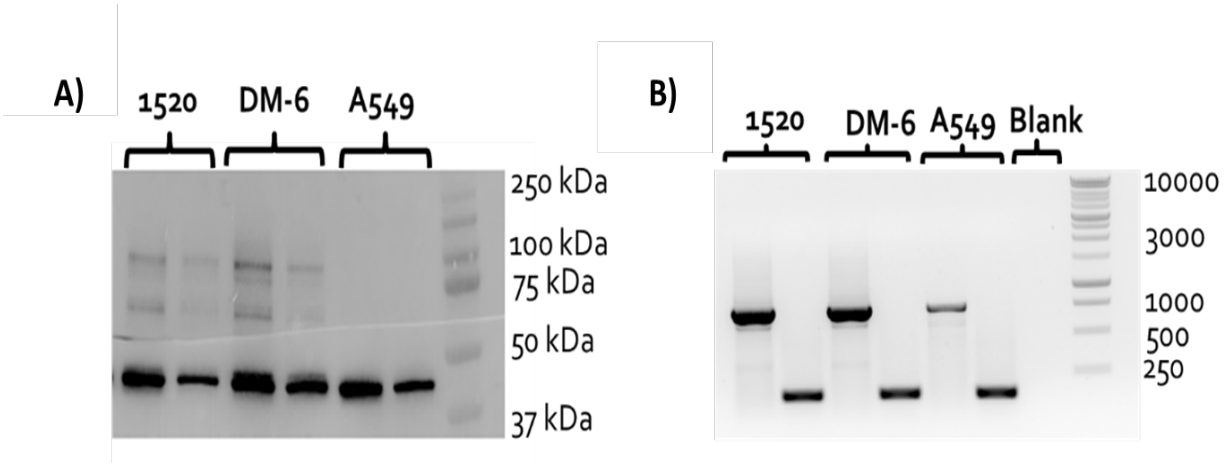

Figure 10: gp100 expression: A) Western blot for assessing of gp100 protein content in 3 cancer cell lines: DM-6, 1520 and A549. β-actin was served as a control (42 kDa). Proteins are represented at two concentrations: 6 (right) and 12 μg (left) for each cell line. **B)** RT-PCR: gp100 (751 bp) expression presented in 1520, DM-6 and A549 cell lines, β-actin served as a control (157 bp).

3.1.7. Cellular uptake of T-MNPs

The cellular uptake of nanoparticle was evaluated on DM-6 (gp100-containing melanoma), 1520 (gp100-containing melanoma), A549 (lung cancer, no gp100 antigen) cell lines. For uptake studies, fluorescent dye (Coumarin 6) loaded NPs were used. PLGA-Coumarin-6 NPs were prepared using a standard single emulsion (O/W) technique and were further used to prepare MNPs. To analyze how different NP to membrane weight ratio would affect uptake of MNPs with 1:0.5, 1:1, and 1:2 ratios were utilized. Such ratios were prepared for D-MNPs and T-MNPs. The results demonstrated that T-MNPs displayed significantly higher uptake compared to the negative control, D-MNPs (Figure 11) in gp100-presenting melanoma cell lines. Moreover, D-MNPs and T-MNPs showed no difference in uptake by lung cancer cell line A549 (no gp100 antigen).

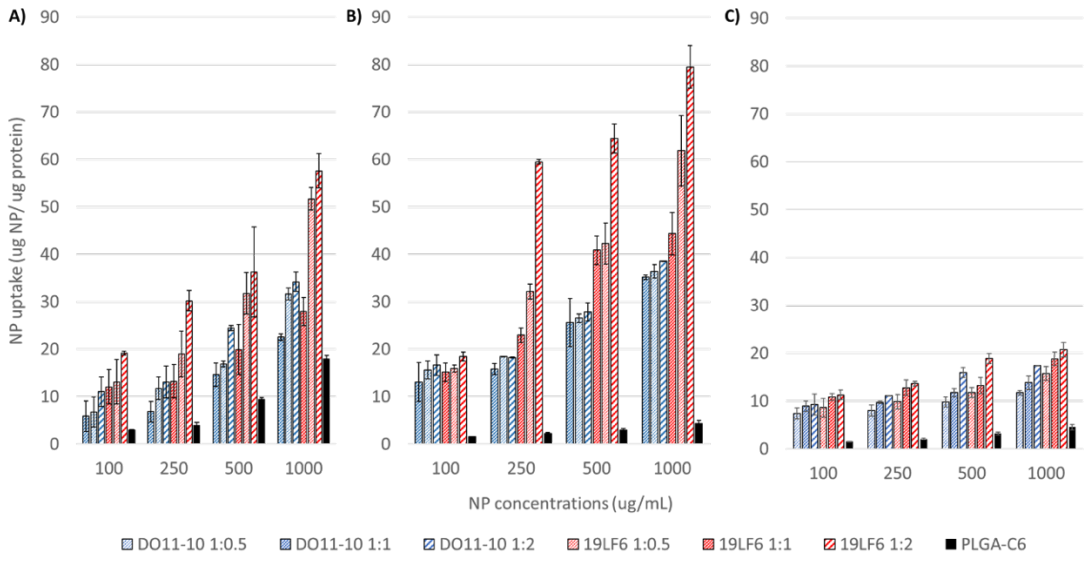

Figure 11: **Cellular uptake:** Uptake of D-MNPs, T-MNPs and PLGA NPs (PLGA-C6) are presented at varying NP to membrane protein weight ratios. MNPs were loaded with a fluorescent dye, Coumarin 6. DM-6, 1520 and A549 cell lines were treated with MNPs for 2 hours. Cell lysates were analyzed for MNP content using a UV-vis Spectrophotometer and cellular uptake was normalized with total cellular protein. Uptake by: **A)** DM-6 **B)** 1520 **C)** A549 cell lines (n=3).

3.1.8. Therapeutic and pharmacokinetics study

The IC50 values of Trametinib were calculated to be approximately 29.3 μg/mL and 1.66 μg/mL for 1520 and DM-6 cell lines, respectively (Figure 12). The therapeutic potential of the Trametinib-loaded T-MNPs was evaluated on both 1520 and DM-6 cell lines. It was shown that T-MNPs had a significantly higher therapeutic efficiency on both melanoma cell lines when compared to the negative controls, specifically at IC50 and IC75 drug concentrations (Figure 13).

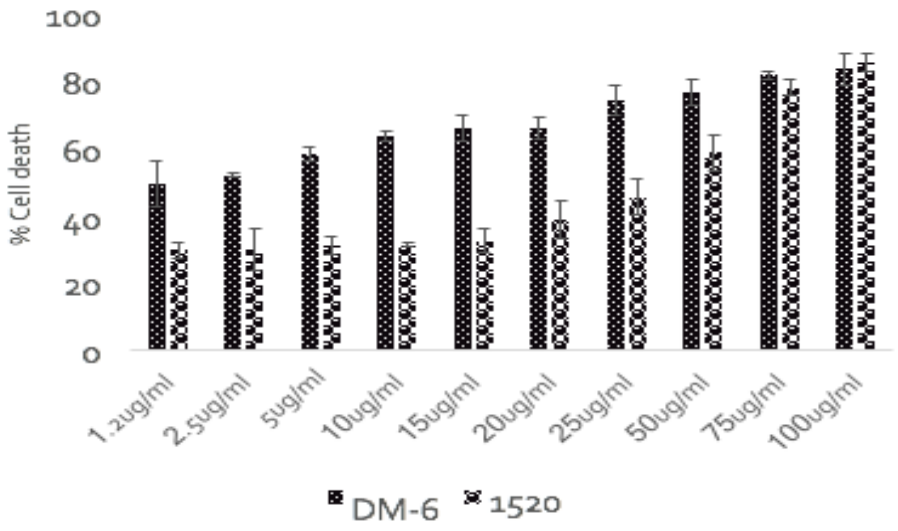

Figure 12: <u>Pharmacokinetic of trametinib</u>: % Viability of DM-6 and 1520 cell lines after 72-hour exposure to free trametinib at ranging concentrations: 1.2 μg/mL -100 μg/mL. Cell viability was measured using MTS assays (n=3).

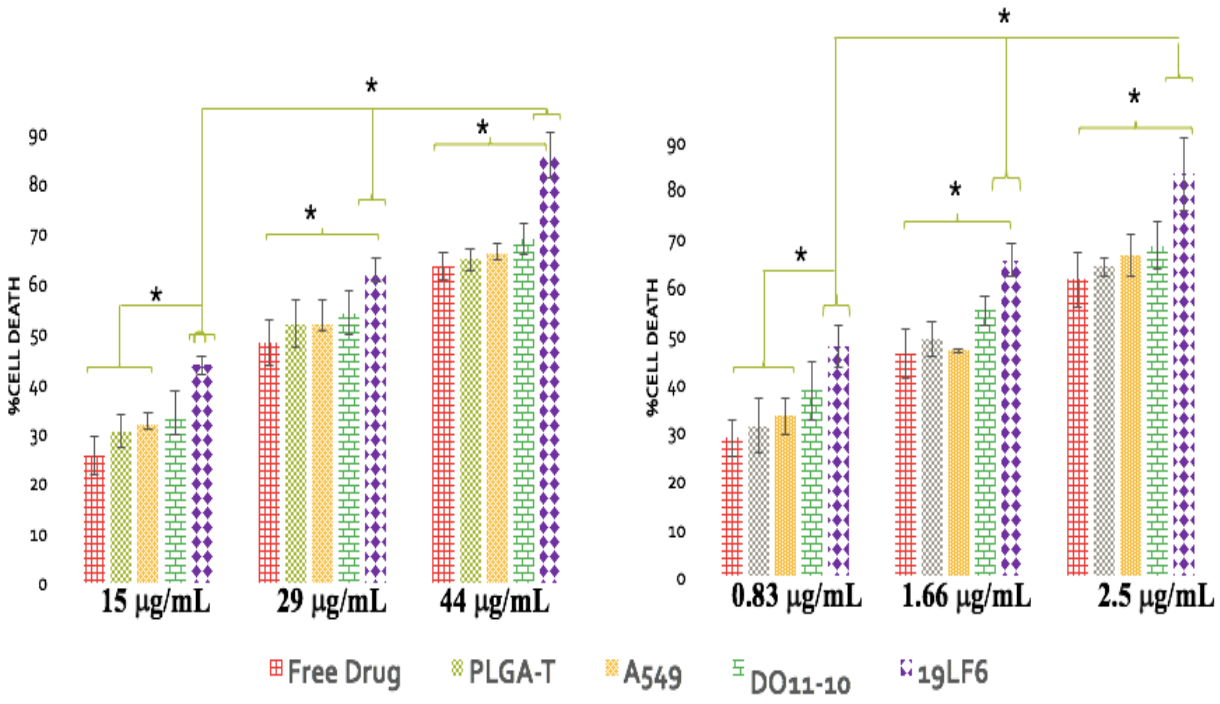

Figure 13: **Therapeutic efficiency:** Therapeutic capabilities of T-MNPs, D-MNPs, A-MNPs, NNPs and free Trametinib on **A)** 1520 and **B)** DM-6 melanoma cell lines. Cell were exposed to these nanoparticle suspensions for 72 hours, and cell viability was evaluated using MTS assays (n=3).

3.1.9. Cyto-compatibility study

The viability of HDF cells was evaluated after interaction with the T-MNPs and PLGA NPs (naked NPs, NNPs) at various concentrations for 24 hours. Since PLGA is FDA approved and biocompatible polymer, T-MNPs were compared to NNPs. The result illustrated that T-MNPs maintained cyto-compatibility up to 1000 µg/mL, similarly to PLGA NPs (NNPs) (Figure 14).

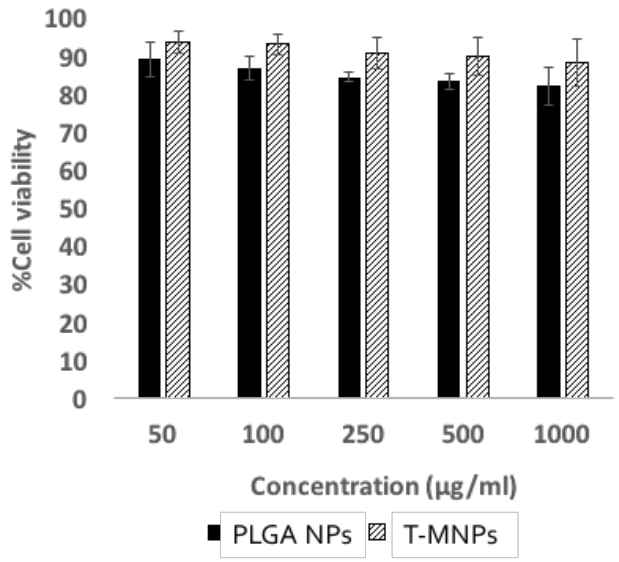

Figure 14: <u>Cyto-compatibility of T-MNPs</u>: Cyto-compatibility of T-MNPs was analyzed on human dermal fibroblast (HDF) at varying NPs concentrations (50 µg/mL -1000 µg/mL) for 24 hours and quantified using MTS assays (n=3).

3.1.10. Hemolysis and blood clotting studies

Blood clotting assay was performed to elucidate potential blood clotting interferences by 19LF6 T-MNPs. The coagulation time of blood in presence of 19LF6 T-MNPs was examined at different time-points: 10, 20, 30 and 60 min. Blood coagulation initiates by activation of a cascade of coagulation factors and surface mediated reactions (36). At all the tested time-points 19LF6 T-MNPs did not display a significantly different blood clotting pattern when compared to that of the saline control (Figure 15.A).

Hemolysis study was also performed to test 19LF6 T-MNPs against potential negative effects on red-blood cells. According to the criterion in the ASTM E2524-08 standard, the test material will cause damage to the red blood cells when the hemolysis is more than 5% percentage. 19LF6 T-

MNPs showed hemolysis properties lower than 5% up to 1000 μg/mL concentration (Figure 15.B). Thus, T-MNPs were considered as hemo-compatible.

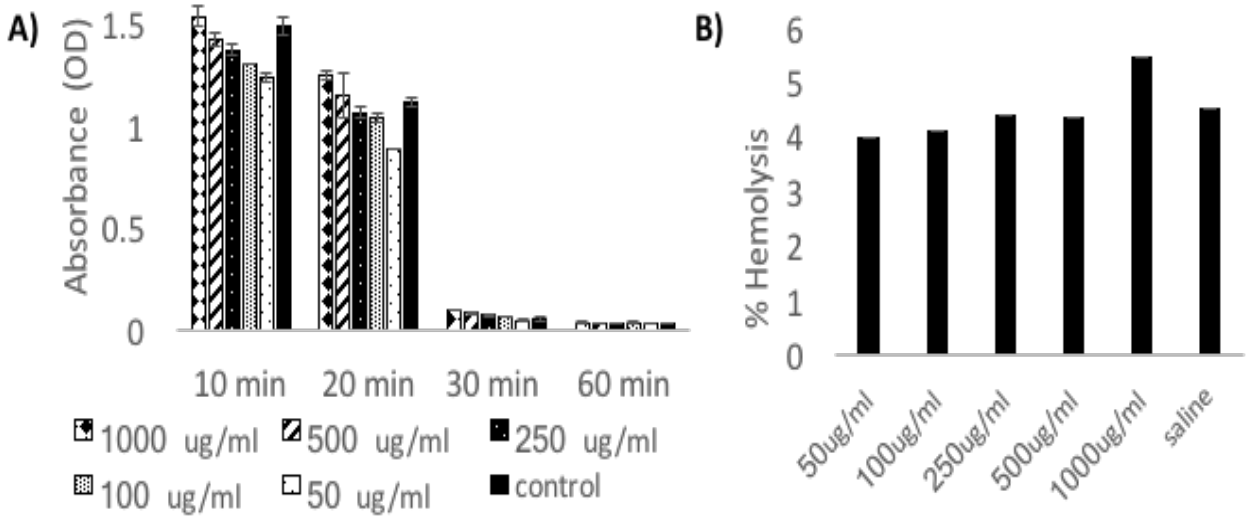

Figure 15: <u>Hemo-compatibility:</u> A) T-MNP influence on blood clotting kinetics; Clotting efficiency was measured in absorbance units (OD) of the supernatants collected from T-MNP- blood samples at pre-determined time-points: 10, 20, 30 and 60 min. The absorbances were quantified using a UV-vis Spectrophotometer. **B)** Hemolysis of blood cells by T-MNP particles was quantified often by measuring sample absorbance at 540 nm. T-MNP nanoparticles were incubated with blood samples for 2 hrs. at 37 C. (n=3)

3.2. Discussion

Characterization of the T-MNPs. The zeta potential of the T-MNPs was approximately -36 mV. The size of the T-MNP particles was monitored using DLS and was found to be 193 ± 56 nm (Figure 7B), with approximately a 20-nm increase compared to the NNPs (172±76 nm). Moreover, transmission electron microscope images of T-MNPs revealed a clear core-shell appearance of the nanostructures (Figure 7A). The stability of the T-MNPs in 0.90% saline solution was found to be

similar across different NP weight to membrane protein weight (w/w) ratios up to two days (Figure 7C). *Ronnie et al.* (28) reported a similar observation. In this study, B16-F10 cancer-coated PLGA nanoparticles were formulated and used for homotypic targeting of breast cancer cells and antigen presentation to immune cells simultaneously. These cancer cell membrane-coated PLGA nanoparticles were found to be approximately 110 nm in size when compared to 80-90 nm naked PLGA NPs. Similar to results of our stability study, they found the stability of the cancer cell membrane coated particles remained constant up to 15 days across a wide range of NP to membrane protein weight ratios: from 1:0.5 to 1:4.

T-MNPs were predicted to retain cell membrane antigens and receptors extracted from 19LF6 cell line. *Zhong et al.* (35) previously defined the 19LF6 cell line to contain a metastatic melanoma antigen, gp100 (209-217)- specific T-cell receptor. Compared to the unstained and isotype controls, stained T-MNP samples with anti-TCR β chain antibody showed a significant, 3-fold higher mean fluorescence intensity (Figure 8A). Such result confirmed the presence of TCR β chain in the T-MNP formulation. To identify the specific anti-gp100 TCR receptor in the T-MNPs formulations, the particles were stained with a custom-made APC-gp100/HLA-A2 complex/refold. Compared to the unstained control, stained T-MNP samples displayed a significant, 15-fold higher mean fluorescence intensity (Figure 8B). These results not only confirmed the presence of the specific TCR, but also its ability to bind to its specific target, previously described by *Zhong et al* (35).

Following the identification of anti-gp100 TCR receptor presence on T-MNPs, its binding kinetics with gp100 were also observed. *Zhong et al.* (35), similarly described the kinetics of these TCR-receptors and defined their affinity constant (KD= 1.4 μM) against a gp100/HLA-A2 tetramer

complex. Using ResoSens label-free optical system, the particles were tested on two different complexes: specific gp100/HLA-A2 and non-specific bGIGL/ HLA-A2 complexes. D-MNPs (1:2 NP to membrane protein ratio weight), was used as a negative control. The binding kinetics were evaluated at 1 min, 30 min and post-wash. Post-wash was performed by washing out the MNP samples and observing the kinetics of bound-only nanoparticles. At post-wash, 250 μg/mL and 500 μg/mL T-MNPs (at 1:2 ratio of NP to membrane protein weight) displayed a statistically significant resonance shift compared to the negative control. Moreover, none of the groups showed significantly different binding characteristics with the bGIGL/ HLA-A2 complex.

The loading efficiency of the T-MNPs was observed to be approximately 61%, and the drug release kinetics displayed an initial burst release followed by a sustained release up to 28 days. The rate of release kinetics differed across the three ratios of NP to membrane protein (w/w) T-MNPs. When comparing T-MNPs and NNPs, it can be clearly seen that cloaking of drug loaded PLGA nanoparticles with T-cell membrane reduced the drug release rates, especially those coated with higher amounts of the cell membrane. This reduction has also been observed in nanoparticles cloaked with membranes from erythrocytes (39). In this study, erythrocyte membrane-coated nanoparticles showed slow release compared to bare nanoparticles. *Aryal et al.* (39) attributed this effect to the membrane's ability to act as a diffusion barrier to provide better sustained drug release, as compared with PEG-based nanoparticles, thereby enhancing the therapeutic efficacy of the drug in acute myeloid leukemia cells.

***In vitro* properties of T-MNPs.** To verify and quantify the presence of gp100 antigen on the DM-6 and 1520 melanoma cell lines, as well as A549, western blotting and RT-PCR studies were carried out. For DM-6 cell line, % relative quantity of the gp100 antigen was found to be almost

2-fold more than the 1520 cell line (Figure 10A). The difference in expression level of the gp100 gene between the two cell lines was not found to be significant (Figure 10B). A549, portrayed a low gp100 expression, approximately 4-fold lower than that of DM-6 and 1520, and no apparent protein presence. However, as it was previously described by *Weidanz et al.* (40), the antigen expression and presentation/lifetime are not always directly related.

Anti-gp100 TCR influence on T-MNP cellular uptake was observed in DM-6 and 1520 melanoma cell lines. Since A549 lung cell lines did not show any apparent gp100 presentation, A549 was used as a negative control cell line. The uptake of T-MNPs at all ratios was significantly higher than that of D-MNPs, the negative control nanoparticles (Figure 11). The uptake of the T-MNPs increased with increasing concentration and was enhanced in the 1520 cell line when compared to that of DM-6 cell line. On the other hand, A549 did not show any selectivity toward T-MNPs or D-MNPs when compared to that of PLGA NPs (NNP) control. Such result was expected due to the absence of the gp100 antigen on A549 cells. The enhanced 1520 uptake of the T-MNPs might have been due to its ability to a better present gp100/ HLA-A2 complex protein compared to that of the DM-6 cell line (40).

Therapeutic efficiency of T-MNPs was then evaluated. *Roller et al.* (16) previously defined the IC50, or the inhibitor concentration at 50% cell viability, for trametinib in the DM-6 cell line. Our result for IC50 values of trametinib for DM-6 and 1520 were found to be approximately 29 μg/mL and 1.6μg/mL, respectively. These values were similar to the previous study from *Roller et al.* (16); however, the IC values often depend on numerous human and in-house factors, therefore, they must be performed for each study. To test the therapeutic efficiency of T-MNPs, DM-6 and 1520 melanoma cancer cells were used. T-MNPs were found to be significantly more efficient

than any of other groups; D-MNPs, A-MNPs, NNPs and free trametinib at the same concentration. Recent studies showed that bare PLGA NPs have limitations owing to nonspecific targeting, and result in uncontrolled tissue distribution of the drug (27). Cell membrane derived ghosts can be used to improve immune evasion, target specificity and drug efficacy (39). Fang et al., surface engineered PLGA NPs with platelet-membrane-derived vesicles since platelet cells have a natural ability to adhere to injured blood vessels as well as circulating pathogens. Such membrane coating provided the particles with a natural platelet-like targeting functions (31). In another study, *Krishnamurthy et al*. showed that the monocyte-membrane vesicle surface engineering of DOX-loaded PLGA NPs resulted in higher cytotoxicity in MCF-7 breast cancer cells compared to that of bare NPs.

Safety of T-MNPs. The T-MNPs were cyto-compatible up 1000 μg/mL concentration. T-MNP cyto-compatibility was compared the cyto-compatibility of NNPs. Overall, T-MNPs were shown to be at least as cyto-compatible as NNPs, or bare PLGA NPs. Similar to our studies, *Guo et al.* (42), likewise, demonstrated that erythrocyte-membrane coated PLGA nanoparticles possessed a similar cyto-compatibility compared to bare PLGA nanoparticles.

T-MNPs were also tested for blood clotting and hemolytic properties. T-MNPs blood clotting characteristics were compared to the saline control and found to have no significant effect on the blood clotting cascade up to 1000 μg/mL. According to the criterion in the ASTM E2524-08 standard, percent hemolysis > 5% is considered toxic to red blood cells (43). T-MNPs-induced blood hemolysis was observed to be < 5% up to 500 μg/mL. Although T-MNPs were found to be toxic to red blood cells at a concentration of 1000μg/mL, such high concentrations of the particles were not used for these studies.

CHAPTER 4

CONCLUSIONS, LIMITATIONS, AND FUTURE WORK

In brief, Trametinib loaded PLGA nanoparticles coated with T cell membrane were successfully synthesized. These membranes coated NPs displayed a high drug encapsulation efficiency of 61% and could release the drug in a sustained fashion over a period of 28 days. The drug release kinetics were found to be dependent on the NP to membrane ratio with the highest membrane content providing the slowest release. It was proposed that the membrane acted as a diffusion barrier. These T-MNPs were promising in terms of optimal size (< 200 nm), stability at physiological conditions, cyto-compatibility (up to 1000 μg/mL) and hemo-compatibility (up to 500μg/mL).

Moreover, the data collected from binding and cellular uptake studies showed that T-MNPs illustrated superior binding and uptake kinetics attributed to their anti-gp100 TCR. These particles showed selective and effective binding to gp100 carrying melanoma cells when compared to that of D-MNPs made from negative T-cell control. Such findings also correlated with enhanced therapeutic efficiencies of T-MNPs. Their cancer killing efficiencies were alignment with binding and uptake characteristics. Particles with the higher membrane content (greater anti-gp100 TCR content) showed to be more effective when compared to that of the lower NP to membrane ratio. Therefore, membrane coated NP system could be a promising carrier that may improve the therapeutic outcomes of melanoma cancer treatments.

In conclusion, the successfully formulated, trametinib-loaded T-MNPs showed superior targeting capabilities towards skin cancer cells and increased the therapeutic efficiency. Based on *in vitro* studies, they could potentially be used to improve chemotherapeutic treatment of melanoma.

Even though the characterization and *in vitro* studies displayed positive results, we do recognize

certain limitations.

- In preparation of these particles, large amount of cells were necessary to provide enough membrane protein for each type of NPs.
- Due to multiple washes of the cell extracts, much of the target proteins could have been lost in the process. Future studies will involve with the optimization of cell extraction protocols.

Future work for this project will include the following studies

- The therapeutic potential of T-MNPs in *in vivo* will be evaluated using animal models (mice).
- T-MNPs will be formulated using T-cells isolated from melanoma patients.

REFERENCES

1. Eggermont AM, Spatz A, Robert C. Cutaneous melanoma. Lancet 2014;383(9919):816-27.
2. Garbe C, Peris K, Hauschild A, Saiag P, Middleton M, Spatz A, et al. Diagnosis and treatment of melanoma: European consensus-based interdisciplinary guideline. Eur J Cancer 2010; 46(2):270-83.
3. Garbe C, Hauschild A, Volkenandt M, Schadendorf D, Stolz W, Reinhold U, et al. Evidence and interdisciplinary consense-based German guidelines: diagnosis and surveillance of melanoma. Melanoma Res 2007;17(6):393-9.
4. Garbe C, Hauschild A, Volkenandt M, Schadendorf D, Stolz W, Reinhold U, et al. Evidence-based and interdisciplinary consensus-based German guidelines: systemic medical treatment of melanoma in the adjuvant and palliative setting. Melanoma Res 2008;18(2):152-60.
5. Dummer R, Guggenheim M, Arnold AW, Braun R, von Moos R. Updated Swiss guidelines for the treatment and followup of cutaneous melanoma. Swiss Med 2011; 141:13320.
6. Leiter U, Garbe C. Epidemiology of melanoma and nonmelanoma skin cancerdthe role of sunlight. Adv Exp Med Biol 2008; 624:89-103
7. Marsden JR, Newton-Bishop JA, Burrows L, Cook M, Corrie PG, Cox NH, et al. Revised U.K. guidelines for the management of cutaneous melanoma 2010. Br J Dermatol 2010; 163(2):238-56.
8. Saiag P, Bosquet L, Guillot B, Verola O, Avril MF, Bailly C, et al. Management of adult patients with cutaneous melanoma without distant metastasis. 2005 update of the French

standards, options and recommendations guidelines. Summary report. Eur J Dermatol 2007;17(4):325-31.

9. Ferlay J, Steliarova-Foucher E, Lortet-Tieulent J, Rosso S, Coebergh JW, Comber H, et al. Cancer incidence and mortality patterns in Europe: estimates for 40 countries in 2012. Eur J Cancer 2013;49(6):1374-403.
10. Bauer J, Garbe C. Acquired melanocytic nevi as risk factor for melanoma development. A comprehensive review of epidemiological data. Pigment Cell Res 2003;16(3):297-306.
11. Whiteman DC, Pavan WJ, Bastian BC. The melanomas: a synthesis of epidemiological, clinical, histopathological, genetic, and biological aspects, supporting distinct subtypes, causal pathways, and cells of origin. Pigment Cell Melanoma Res 2011; 24(5):879-97.
12. Wheatley K, Wilson JS, Gaunt P, Marsden JR. Surgical excision margins in primary cutaneous melanoma: a meta-analysis and Bayesian probability evaluation. Cancer Treat Rev 2016; 42: 73-81.
13. Hayes AJ, Maynard L, Coombes G, Newton-Bishop J, Timmons M, Cook M, et al. Wide versus narrow excision margins for high-risk, primary cutaneous melanomas: long-term follow-up of survival in a randomised trial. Lancet Oncol 2016; 17(2):184-92
14. Skin cancer infographics. Retrieved March 14, 2017, from https://www.dreamstime.com/stock-illustration-skin-cancer-infographics-melanoma-medical-infographic-set-icons-other-elements-image62166433
15. Mocellin S, Pasquali S, Rossi CR, Nitti D. Interferon alpha adjuvant therapy in patients with high-risk melanoma: a systematic review and meta-analysis. J Natl Cancer Inst 2010; 102(7):493-501.

16. Roller, Devin G., Brian Capaldo, Stefan Bekiranov, Aaron J. Mackey, Mark R. Conaway, Emanuel F. Petricoin, Daniel Gioeli, and Michael J. Weber. "Combinatorial drug screening and molecular profiling reveal diverse mechanisms of intrinsic and adaptive resistance to BRAF inhibition in V600E BRAF mutant melanomas." *Oncotarget*. Impact Journals LLC.
17. Welcome to the Department of Surgery. (n.d.). Retrieved March 14, 2017, from http://www.ucdenver.edu/academics/colleges/medicalschool/departments/surgery/divisions/GITES/Types-of-Surgery/Pages/Melanoma.aspx
18. Guo J, Si L, Kong Y, Flaherty KT, Xu X, Zhu Y, et al. Phase II, open-label, single-arm trial of imatinib mesylate in patients with metastatic melanoma harboring c-Kit mutation or amplification. J clin Oncol 2011;29(21):2904-9.
19. Hauschild A, Rosien F, Lischner S. Surgical standards in the primary care of melanoma patients. Onkologie 2003;26(3): 218-22.
20. Thompson JF, Shaw HM. Sentinel node mapping for melanoma: results of trials and current applications. Surg Oncol Clin N Am 2007;16(1):35-54
21. Lugowska I, Paterczyk H., Kozak K., Rutkowski P., Trametinib: a MEK inhibitor for management of metastatic melanoma, 2015, 8: 2251-2259.
22. Tran, Eric, Simon Turcotte, Alena Gros, Paul F. Robbins, Yong-Chen Lu, Mark E. Dudley, John R. Wunderlich, Robert P. Somerville, Katherine Hogan, Christian S. Hinrichs, Maria R. Parkhurst, James C. Yang, and Steven A. Rosenberg. "Cancer Immunotherapy Based on Mutation-Specific CD4 T Cells in a Patient with Epithelial Cancer." *Science*. American Association for the Advancement of Science, 2014; 344:641-645.
23. "CAR T-Cell Immunotherapy for ALL." *National Cancer Institute*. Available from: https://www.cancer.gov/about-cancer/treatment/research/car-t-cells

24. Pinto-Alphandary H, Andremont A, Couvreur P. Targeted delivery of antibiotics using liposomes and nanoparticles: research and applications. Int J Antimicrob Agents 2000;13:155–168.
25. Xie, Jin, Seulki Lee, and Xiaoyuan Chen. "Nanoparticle-based theranostic agents." *Advanced drug delivery reviews*. U.S. National Library of Medicine 2010; 62(11): 1064-1079.
26. Yuan, Weien, Yunpeng Cai, Mingxin Xu, Minglu Yuan, and Zhenguo Liu. "Developments in human growth hormone preparations: sustained-release, prolonged half-life, novel injection devices, and alternative delivery routes." *International Journal of Nanomedicine* 2014; 9: 3527-3538.
27. Danhier F., Eduardo A., Joana M., Régis C., Aude L., and Véronique P. "PLGA-based nanoparticles: An overview of biomedical applications." *Journal of Controlled Release* 2012; 161(2): 505-22.
28. Fang RH, Hu CM, Luk BT, et al. Cancer cell membrane-coated nanoparticles for anticancer vaccination and drug delivery. Nano Lett. 2014;14(4):2181–2188
29. Tan S. et al., Cell or Cell Membrane-Based Drug Delivery Systems, Theranostics, 2015; 5(8): 863-881
30. Parodi, A.; Quattrocchi, N.; van de Ven, A. L.; Chiappini, C.; Evangelopoulos, M.; Martinez, J. O.; Brown, B. S.; Khaled, S. Z.; Yazdi, I. K.; Vittoria Enzo, M.; et al. Synthetic Nanoparticles Functionalized with Biomimetic Leukocyte Membranes Possess Cell-Like Functions. Nat. Nanotechnol. 2013, 8, 61–68.
31. Hu, Q. Y.; Sun, W. J.; Qian, C. G.; Wang, C.; Bomba, H. N.; Gu, Z. Anticancer Platelet-Mimicking Nanovehicles. Adv. Mater. 2015, 27, 7043−7050.

32. Foth M., Jasper W., Ciaran D., Peter D., and William M. "Prognostic and predictive biomarkers in melanoma: an update." *Expert Review of Molecular Diagnostics* 2015;16(2): 223-237.

33. Heslop, H. E. "Genetic engineering of T-cell receptors: TCR takes to titin." *Blood* 2013; 122(6): 853-54.

34. Girotti MR, Marais R. Déjà vu: EGF receptors drive resistance to BRAF inhibitors. *Cancer Discov*. 2013;3(5):487–490.

35. Zhong S., Karolina M., Laura A. J., Zhiya Y., Eleazar Vega-Saenz De M., Farbod D., Katelyn M., Kevin H., Josh B., Emily C., Yongzhao S., Steven A. R., Nicholas P. R., Iman O., and Michelle K. "T-cell receptor affinity and avidity defines antitumor response and autoimmunity in T-cell immunotherapy." *Proceedings of the National Academy of Sciences of the United States of America*. National Academy of Sciences, 23 Apr. 2013; 110(17): 6973-6978.

36. Yildirim, Adem, Erol Ozgur, and Mehmet Bayindir. "Impact of mesoporous silica nanoparticle surface functionality on hemolytic activity, thrombogenicity and non-specific protein adsorption." *Journal of Materials Chemistry B* 1.14 (2013): 1909. Web.

37. Farokhzad O., Nanotechnology: Platelet mimicry, Nature, 2014; 14(4), 2181-2188.

38. Arrangoiz R., Joel D., Fernando C., Manuel M., Eduardo M., and Enrique L. "Melanoma Review: Epidemiology, Risk Factors, Diagnosis and Staging." *Journal of Cancer Treatment and Research*. Science Publishing Group, 21 Apr. 2016; 4: 1-15

39. Hu, C. M. J.; Zhang, L.; Aryal, S.; Cheung, C.; Fang, R. H.; Zhang, L. F. Erythrocyte Membrane-Camouflaged Polymeric Nano- particles as a Biomimetic Delivery Platform. Proc. Natl. Acad. Sci. U. S. A. 2011, 108, 10980−10985.

40. Weidanz, J. A., T. Nguyen, T. Woodburn, F. A. Neethling, M. Chiriva-Internati, W. H. Hildebrand, and J. Lustgarten. "Levels of specific peptide-HLA class I complex predicts tumor cell susceptibility to CTL killing." *Journal of immunology (Baltimore, Md. : 1950)*. U.S. National Library of Medicine, 2006; 177(8):5088-97
41. Krishnamurthy S, Gnanasammandhan MK, Xie C, Huang K, Cui MY, Chan JM. Monocyte Cell Membrane-derived Nanoghosts for Targeted Cancer Therapy. Nanoscale. 2016;8(13):6981–5. doi: 10.1039/C5NR07588B.
42. Guo Y. et al., Erythrocyte Membrane-Enveloped Polymeric Nanoparticles as Nanovaccine for Induction of Antitumor Immunity against Melanoma. ACS Nano, 2015; 9(7): 6918-6933.
43. "E2524-08 Standard Test Method for Analysis of Hemolytic Properties of Nanomaterials." E2524-08 Standard Test Method for Analysis of Hemolytic Properties of Nanoparticles. Available from: https://www.astm.org/Standards/E2524.htm

BIOGRAPHICAL INFORMATION

Gizem Oter was born in Ankara, Turkey on June 5, 1991. She graduated from Firat University with a Bachelor Degree in Bioengineering in 2013 in Elazig, Turkey. She was elected to be a scholar of Turkish Republic Ministry of National Education. She started her Master research program at the University of Texas at Arlington (UTA) in 2015 under the supervisor of Dr. Kytai T. Nguyen. During the time in Dr. Kytai T. Nguyen's and Dr. Jon Weidanz's laboratories, she had the pleasure of working on several projects in the field of nanoparticulate immunotherapy. She intends on continuing the work with nanoparticle-based drug delivery platforms and tissue engineering in the future.